Fine structure of the beryllium ^3P states calculated with all-electron explicitly correlated Gaussian functions

Monika Stanke[*] and Andrzej Kędziorski[†]
Institute of Physics, Faculty of Physics, Astronomy, and Informatics, Nicolaus Copernicus University, ul. Grudziądzka 5, Toruń, PL 87-100, Poland

Ludwik Adamowicz[‡]
Department of Chemistry and Biochemistry and Department of Physics, University of Arizona, Tucson, Arizona 85721, USA and Centre for Advanced Study, N-0271 Oslo, Norway

(Received 9 October 2021; accepted 24 December 2021; published 18 January 2022)

The recently presented general algorithm for calculating an atomic fine structure [Kędziorski *et al.*, Chem. Phys. Lett. **751**, 137476 (2020)] is employed to study the fine splitting of the lowest eight ^3P states of beryllium, i.e., the $1s^2\ 2s\ np, n = 2, \ldots, 9, {}^3P$ states. All-electron explicitly correlated Gaussian functions and a finite-nuclear-mass variational method are used in the calculations. The energies of the states are augmented with the leading α^2 relativistic and α^3 (and approximate α^4) QED corrections ($\alpha = \frac{1}{c}$ is the fine-structure constant, and c is the speed of light in atomic units). The calculated results are compared with the available experimental data.

DOI: 10.1103/PhysRevA.105.012813

I. INTRODUCTION

Experimental spectra of small atomic systems are an important area of comparison between very high resolution measurements and state-of-the-art quantum-mechanical calculations. There are constant improvements being made to the databases that list the most current atomic experimental data concerning atomic interstate transitions [1]. There is also constant progress being made in high-accuracy calculations of atomic energy levels. Among those levels, lines resulting from the splitting of the main atomic lines due to spin-orbit (SO) magnetic interactions are particularly interesting, as they provide fingerprint signatures that are characteristic of specific atomic systems. This splitting that arises from the interaction of the orbital motion of the electrons with the electronic spins gives rise to the fine structure of the spectral lines of atoms with nonzero total orbital angular momenta and nonzero total spin angular momenta.

The most accurate theoretical calculations of atomic fine structures have been performed for two- and three-electron atoms using Hylleraas-type explicitly correlated functions (see, for example, the calculations for the spectra of the lithium atom by Wang *et al.* [2], as well as the calculations for other two- and three-electron atomic systems [3–7]). However, extending the use of Hylleraas functions to expand wave functions of atoms with more than three electrons has been hampered by technical difficulties with calculating the Hamiltonian matrix elements [8].

An alternative type of explicitly correlated basis function that has been gaining popularity in high-accuracy atomic calculations, especially for atoms with more than three electrons, is the set of all-electron explicitly correlated Gaussian functions (ECGs). These functions exponentially depend on squared distances between electrons of all electronic pairs in the system. For four- and five-electron atomic systems, the use of ECGs enabled achieving very high accuracy in calculations of interstate transitions [9–17]. The popularity of ECGs in atomic calculations results from the high efficiency of these functions in describing the correlated motion of the electrons and from the relative simplicity of the algorithms for calculating the Hamiltonian matrix elements with these functions. These algorithms can be analytically derived and coded in a general form for an arbitrary number of electrons in the atom. One can also easily derive algorithms for calculating the first derivatives of the Hamiltonian matrix elements with respect to the ECG nonlinear parameters and use them to determine the energy gradient [18,19]. The use of the gradient in the variational energy minimization considerably accelerates the minimization process and enables achieving high accuracy in the calculations. It also allows extending the size of atomic systems whose spectra can be very accurately calculated using present-day computer systems. As the computational time in ECG atomic calculations scales as the factorial of the number of electrons in the system, the practical present limit of the number of electrons in the atom that can be calculated with high accuracy is less than 10. The largest atomic system considered so far in ECG calculations is carbon and nitrogen atoms [20–23]. Calculations for larger atoms will need to wait for a new generation of computer hardware to be performed at the same accuracy level which is now possible for four- and five-electron atoms.

The advantage of using ECGs in atomic calculations also stems from the fact that matrix elements involving operators representing the leading relativistic and QED corrections can be analytically evaluated in a compact form. These matrix

[*]monika@fizyka.umk.pl
[†]andrzej.kedziorski@fizyka.umk.pl
[‡]ludwik@email.arizona.edu

elements can be calculated for an arbitrary number of electrons. Including the relativistic and QED corrections in the total state energies of the considered atom, as done in the present work, significantly improves the accuracy of the calculated interstate transition energies.

There are some drawbacks of using ECGs in atomic calculations. They are related to these functions not satisfying Kato's cusp conditions and to their decaying too fast at large distances. However, if a large number of Gaussians is used in the calculation (e.g., in the present calculations of the lowest eight beryllium ^{3}P states we use 10 000–11 000 ECGs for each state) and the Gaussian exponential parameters are thoroughly variationally optimized, then the above-mentioned drawbacks can be overcome [9–12]. Such optimization aided by inputting the energy gradient determined with respect to these parameters into the procedure that runs the variational energy minimization is carried out in this work for each of the eight lowest ^3P states of the beryllium atom.

In the approach used in the present calculations, the Hamiltonian representing the internal state of the atom is obtained by separating out the motion of the center of mass from the laboratory-frame nonrelativistic Hamiltonian. The resulting internal Hamiltonian explicitly depends on the mass of the nucleus. Thus, the energy calculated, for example, for the ground state of ^{9}Be is slightly higher than the energy of the beryllium atom with an infinite nuclear mass, $^\infty$Be. Also, the optimization of the exponential ECG parameters is carried out by the minimization of the ^{9}Be energy and not the $^\infty$Be energy, as was done in the standard calculations. After the basis sets are generated for all eight ^3P ^{9}Be states and their optimal total nonrelativistic energies are obtained, they are used to calculate the corresponding $^\infty$Be energies without reoptimization of the exponential parameters. Only the linear expansion parameters are adjusted for the change in the nuclear mass.

In a recent paper, Puchalski *et al.* [24] calculated the fine and hyperfine structures of the $2s3p$ ^3P and $2p^2$ $^3P^e$ states of beryllium. The calculations were performed using ECG basis functions. It is interesting to compare the present variational nonrelativistic energy of the lowest $2s3p$ ^3P state of $^\infty$Be with their best energy for that state, as well as with their energy extrapolated to an infinite number of the basis functions. We expect the comparison to show the advantage of using the gradient-based variational minimization that is employed in the present work. The $^\infty$Be energy and the extrapolated energy reported by Puchalski *et al.* are -14.56724421584 and $-14.567244232(8)$ a.u., respectively. The former energy was obtained using 6144 ECGs. The best variational energy obtained in this work (see Sec. VI) using 10 000 ECGs is -14.567244231 a.u. Clearly, the use of the gradient not only resulted in a noticeably lower energy of the state but also allowed us to generate a significantly larger basis set.

The main goal of this work is to calculate the fine structure of the eight lowest $2snp$, $n = 2, \ldots, 9$, ^3P levels of the beryllium atom. The splitting is calculated using the first order of the perturbation theory. Like the nonrelativistic internal Hamiltonian, the operators representing the leading α^2 relativistic corrections, including the spin-orbit magnetic-interaction correction, explicitly depend on the nuclear mass. The operators are obtained by first expressing them in terms of the laboratory coordinates and then transforming them to a new coordinate system in which the first three coordinates are the laboratory coordinates of the center of mass and the remaining coordinates are the so-called internal coordinates (see the next section). Thus, in the present calculations, the use of the finite-nuclear-mass (FNM) approach makes both the nonrelativistic total energy and the relativistic corrections explicitly dependent on the mass of the nucleus; that is, the so-called recoil effects are accounted for.

The procedure to calculate the atomic fine structure was implemented in our previous work [25]. In that work, as an illustrative example, we showed preliminary calculations for the lowest two ^3P states of beryllium. In the present work, the basis sets for the two states were increased to 10 000 ECGs. Also, the number of considered ^3P states was increased to eight. For the seventh and eighth states, basis sets of 11 000 ECGs are generated. Such large basis sets ensure that very high accuracy is achieved in the calculations.

There have been previous calculations of the fine structure of the beryllium ^{3}P states. They include the works of Fischer and Tachiev [26], Chung and Zhu [27], and Chen [28], as well as the above-mentioned recent work of Puchalski *et al.* [24]. In the latter work, only the lowest ^3P state of beryllium was considered. Due to the use of large ECG basis sets in the present work and the consideration of the eight lowest beryllium ^3P states, the present calculations represent, in our view, significant progress over the previous works. This view is enforced by the favorable comparison of the present results with the available experimental data [1].

II. THE NONRELATIVISTIC CALCULATIONS

The procedure used in the present work to calculate the total energies, transitions energies, and fine-structure splitting was presented in our recent paper [25]. Here, only a short summary of the approach is presented.

In the first step of the procedure, the nonrelativistic energies and the corresponding wave functions of the considered states are calculated. The calculations are performed without assuming the Born-Oppenheimer (BO) approximation and involve an internal Hamiltonian that, as mentioned, is obtained from the laboratory-frame full Hamiltonian by separating out the center-of-mass motion. In general, for an atom with n electrons, the separation is done by expressing the laboratory-frame $3(n+1)$-dimensional Hamiltonian in terms of new coordinates, of which the first three are Cartesian laboratory-frame coordinates of the center of mass and the remaining $3n$ coordinates are the internal (Cartesian) coordinates. These coordinates are the coordinates of the vectors $\mathbf{r}_i$ $(i = 1, \ldots, n)$, with the origin at the nucleus and the end at electrons $(i = 1, \ldots, n)$. The laboratory-frame Hamiltonian transformed to the new coordinates rigorously separates into the operator representing the kinetic energy of the center-of-mass motion and the internal operator that has the following form (in atomic units):

$$\hat{\mathrm{H}}_{\mathrm{int}} = -\frac{1}{2}\left(\sum_{i=1}^{n}\frac{1}{\mu_i}\nabla_{\mathbf{r}_i}^T\cdot\nabla_{\mathbf{r}_i} + \frac{1}{m_0}\sum_{\substack{i,j=1\\ i\neq j}}^{n}\nabla_{\mathbf{r}_i}^T\cdot\nabla_{\mathbf{r}_j}\right) + \sum_{i=1}^{n}\frac{q_0 q_i}{r_i} + \sum_{i>j=1}^{n}\frac{q_i q_j}{r_{ij}}, \tag{1}$$

where m_0 is the mass of the nucleus and q_0 is its charge, $q_i = -1$ $(i = 1, \ldots, n)$ are electron charges, and $\mu_i = m_0 m_i/(m_0 + m_i)$ are their reduced masses ($m_i = 1$, $i = 1, \ldots, n$, are the electron masses). One can notice that Hamiltonian (1) describes the motion of n so-called pseudoelectrons that have the same charges as the original electrons, but with their masses replaced by the reduced masses, in the central field of the charge of the nucleus. The motions of the pseudoelectrons are coupled through the Coulombic interactions, $\sum_{i=1}^{n} \frac{q_0 q_i}{r_i} + \sum_{i>j=1}^{n} \frac{q_i q_j}{r_{ij}}$, where $r_{ij} = |\mathbf{r}_j - \mathbf{r}_i|$, and through the so-called mass polarization term, $-\frac{1}{2}\sum_{\substack{i,j=1 \\ i\neq j}}^{n} (1/m_0)\nabla_{\mathbf{r}_i}^T \cdot \nabla_{\mathbf{r}_j}$. The internal Hamiltonian (1) is used in the present variational calculations of the nonrelativistic total energies and the corresponding ground- and excited-state wave functions of the beryllium atom (^{9}Be and $^\infty$Be; obviously, the mass polarization terms vanishes for $^\infty$Be). The nonrelativistic wave functions are also used in the first-order perturbation-theory calculations of the relativistic and QED corrections to the total energies of the considered states.

The spatial parts of the wave functions of the considered ^3P states of beryllium are expanded in terms of the following ECG ($L = 1, M_L = 0$) basis functions:

$$\phi_k^{(L=1)} = z_{i_k} \exp[-\mathbf{r}^T (A_k \otimes I_3)\mathbf{r}], \tag{2}$$

respectively, where electron label i_k varies from 1 to n. A_k in (2) is an $n \times n$ symmetric matrix of the exponential parameters of the Gaussian which is specific to each ECG, $\otimes$ is the Kronecker product, and I_3 is a 3×3 identity matrix. In (2), $\mathbf{r}$ is a $3n$ vector of the internal coordinates of the n pseudoelectrons which has the following form:

$$\mathbf{r} = \begin{pmatrix} \mathbf{r}_1 \\ \mathbf{r}_2 \\ \vdots \\ \mathbf{r}_n \end{pmatrix} = \begin{pmatrix} x_1 \\ y_1 \\ z_1 \\ \vdots \\ x_n \\ y_n \\ z_n \end{pmatrix}. \tag{3}$$

$(A_k \otimes I_3)$ is denoted as $\mathbf{A}_k$.

To ensure that basis functions (2) are square integrable, which they should be since they are used to expand bound states of the beryllium atom, the $\mathbf{A}_k$ matrix has to be made positive definite. In order for this to happen, $\mathbf{A}_k$ is represented in the Cholesky-factored form as $\mathbf{A}_k = (L_k L_k^T) \otimes I_3$, with L_k being a real $n \times n$ lower triangular matrix. Such a representation makes $\mathbf{A}_k$ positive definite for any values of the L_k matrix elements in the $(-\infty, +\infty)$ range. As the L_k matrix elements are the variational parameters that are optimized in the present calculations by the minimization of the energy of the particular state, this optimization can be performed without any constraints. This is always a desirable feature of any optimization.

The spatial part of the wave functions of the considered ^3P states is a linear combination of basis functions (2) with the linear expansion coefficients obtained by solving the corresponding secular equation problem. The solution involves constructing the Hamiltonian and overlap matrices and their simultaneous diagonalization. In the calculation of the Hamiltonian and overlap matrix elements, the proper permutational symmetry has to be implemented for each basis function. We use the spin-free formalism in this implementation. In this formalism, an appropriate symmetry projector is constructed and applied to each basis function to impose the desired symmetry properties of the total wave function. The projector is constructed using the standard procedure involving Young's operators $\hat{Y}$ [29–31]. As the projector commutes with the Hamiltonian, the projector from the bra side of the matrix element can be moved to the ket side $\langle \hat{Y}\Phi_L|\hat{\mathrm{H}}_{\mathrm{int}}|\hat{Y}\Phi_L\rangle = \langle \Phi_L|\hat{\mathrm{H}}_{\mathrm{int}}|\hat{Y}^\dagger\hat{Y}\Phi_L\rangle$, and thus, the projector on the ket side becomes equal to $\hat{Y}^\dagger\hat{Y}$. The procedure used here to generate the permutational symmetry projector was described in our previous work [19].

For the considered ^3P states of the beryllium atom the symmetry projector (Young's operators) can be chosen as

$$\hat{Y}_{^3P} = (\hat{1} - \hat{P}_{13})(\hat{1} - \hat{P}_{14} - \hat{P}_{34})(\hat{1} + \hat{P}_{12}), \tag{4}$$

where $\hat{P}_{ij}$ interchanges the spatial coordinates of the ith and jth electrons. In the beryllium calculation, $\hat{Y}^\dagger\hat{Y}$ contains $4! = 24$ terms. Thus, each matrix element is a sum of 24 different terms (as four of these terms vanish for the ^3P states, the number of terms reduces to 20).

In the calculation of the matrix elements of the operators representing the spin-independent leading relativistic corrections, i.e., the mass-velocity, Darwin, orbit-orbit, and contact spin-spin interaction operators, $\hat{H}_{\mathrm{MV}}$, $\hat{H}_{\mathrm{D}}$, $\hat{H}_{\mathrm{OO}}$, and $\hat{H}_{\mathrm{SSF}}$, the spin-free approach is also used. However, in calculating first-order corrections to the energy of ^3P states due to the (noncontact) spin-spin and spin-orbit interactions, the corresponding operators explicitly depend on the electron spins. Thus, the complete wave function that explicitly includes the electron spin and spatial components, i.e. [32],

$$\Psi_{SM_S LM_L}(\sigma, \mathbf{r}) = \hat{A}[\Omega_{SM_S}(\sigma)\, \Phi_{LM_L}(\mathbf{r})], \tag{5}$$

has to be used. In (5), antisymmetrizer $\hat{A}$ acts on both spatial $\mathbf{r}$ and spin $\sigma = (\sigma_1, \ldots, \sigma_n)$ electron variables. $\Omega_{SM_S}(\sigma)$ is an eigenfunction of the total electron spin operators, $\hat{S}^2$ and $\hat{S}_z$. No permutational properties are imposed on the spatial function $\Phi_{LM_L}(\mathbf{r})$ and the permutation projection of the spin-free approach $Y_{^3P}$ now transforms the spin eigenfunction $\Omega_{SM_S}(\sigma)$ [25]. This eigenfunction has the following form for the ^3P ($S = M_S = 1$) states of beryllium: $\Omega_{11}(\sigma) = \frac{1}{\sqrt{2}}[\alpha(\sigma_1)\beta(\sigma_2) - \beta(\sigma_1)\alpha(\sigma_2)]\alpha(\sigma_3)\alpha(\sigma_4)$. For a practical reason, the calculations of the matrix elements of the spin-dependent operators are performed using the spatial $\Phi(\mathbf{r})_{L=M_L=1}$ wave functions and not $\Phi(\mathbf{r})_{L=M_L=0}$ wave functions. This requires replacing z_{i_k} in Eq. (2) by $-(x_{i_k} + iy_{i_k})/\sqrt{2}$, where $i^2 = -1$. The first-order corrections to the energy are given for the $|(SL)JM_J\rangle$ eigenstates, where $\mathbf{J} = \mathbf{S} + \mathbf{L}$ is the total angular momentum of the electrons.

III. RELATIVISTIC OPERATORS

The operators representing the spin-independent components of the leading relativistic corrections of the order of $\alpha^2 (\propto c^{-2})$ that include the mass-velocity (MV), Darwin (D), and orbit-orbit (OO) terms expressed in terms of the internal

coordinates are

$$\hat{H}_{\rm MV} = -\frac{1}{8}\alpha^2\left[\frac{1}{m_0^3}\left(\sum_{i=1}^{n}\nabla_{\mathbf{r}_i}\right)^4 + \sum_{i=1}^{n}\frac{1}{m_i^3}\,\nabla_{\mathbf{r}_i}^4\right], \tag{6}$$

$$\hat{H}_{\rm D} = -\frac{\pi}{2}\alpha^2\sum_{i=1}^{n}\left[\frac{4}{3}\frac{(g-1)(I+\xi)}{m_0^2} + \frac{1}{m_i^2}\right] q_0 q_i\,\delta^3(\mathbf{r}_i) - \frac{\pi}{2}\alpha^2\sum_{i=1}^{n}\sum_{j\neq i}^{n}\frac{1}{m_i^2}\,q_i q_j\,\delta^3(\mathbf{r}_{ij}), \tag{7}$$

$$\hat{H}_{\rm OO} = -\frac{1}{2}\alpha^2\sum_{i=1}^{n}\sum_{j=1}^{n}\frac{q_0 q_j}{m_0 m_j}\left[\frac{1}{r_j}\nabla_{\mathbf{r}_i}{}^T\cdot\nabla_{\mathbf{r}_j} + \frac{1}{r_j^3}\,\mathbf{r}_j^T\cdot\left(\mathbf{r}_j^T\cdot\nabla_{\mathbf{r}_i}\right)\nabla_{\mathbf{r}_j}\right]$$
$$+\frac{1}{2}\alpha^2\sum_{i=1}^{n}\sum_{j>i}^{n}\frac{q_i q_j}{m_i m_j}\left[\frac{1}{r_{ij}}\nabla_{\mathbf{r}_i}^T\cdot\nabla_{\mathbf{r}_j} + \frac{1}{r_{ij}^3}\,\mathbf{r}_{ij}^T\cdot\left(\mathbf{r}_{ij}^T\cdot\nabla_{\mathbf{r}_i}\right)\nabla_{\mathbf{r}_j}\right]. \tag{8}$$

In the above, $\delta(\mathbf{r})$ is the Dirac delta function, and I and g are the nuclear spin and nuclear g factor, respectively; $\xi = 1/4$ for half-integer I, and $\xi = 0$ otherwise. The above energy corrections uniformly shift all of the $^{2S+1}L_J$ energy levels of a given atomic ^{2S+1}L term. The leading relativistic corrections also include the spin-spin Fermi contact term (SSF) represented by the following operator:

$$\hat{H}_{\rm SSF} = -\frac{8\pi}{3}\alpha^2\sum_{\substack{i,j=1\\ j>i}}^{n}\frac{q_i q_j}{m_i m_j}(\mathbf{s}_i\cdot\mathbf{s}_j)\delta(\mathbf{r}_{ij}). \tag{9}$$

Even though this operator explicitly involves electronic spins $\mathbf{s}_i$, it provides the SSF first-order correction to the energy that does not split the atomic ^{2S+1}L terms.

In the calculations of the spin-dependent relativistic corrections of the order of α^2 the corresponding operators representing the SO and spin-spin (SS) interactions are used. Before they are used in the calculations, the operators, originally expressed in terms of the laboratory coordinates [33], are transformed to the internal coordinate system. Retaining only terms dependent on the internal $\mathbf{r}_i$ coordinates, the following SS operator is obtained:

$$\hat{H}'_{\rm SS} = \alpha^2\sum_{j=1}^{n}\sum_{i>j}^{n}\frac{q_i q_j}{m_i m_j}\left\{(\mathbf{s}_i\cdot\nabla_{\mathbf{r}_i})(\mathbf{s}_j\cdot\nabla_{\mathbf{r}_j})\frac{1}{r_{ij}}\right\}, \tag{10}$$

where $\nabla_{\mathbf{r}_i}$ and $\nabla_{\mathbf{r}_j}$ operate on only $1/r_{ij}$. The above operator includes part of the Fermi-contact operator (9). To separate out this overlapping part, tensor operator techniques [34] are applied. The procedure is explained in our previous paper [25].

The electron spin-orbit interaction $\hat{H}_{\rm SO}$ has the following form:

$$\hat{H}_{\rm SO} = -\alpha^2\sum_{k=1}^{n}\mathbf{s}_k\cdot\left\{\frac{q_0 q_k}{2m_k}\left(\frac{1}{m_k}+\frac{2}{m_0}\right)\frac{1}{r_k^3}(\mathbf{r}_k\times\mathbf{p}_k)\right\}$$
$$+\alpha^2\sum_{k=1}^{n}\mathbf{s}_k\cdot\sum_{\substack{l=1\\ l\neq k}}^{n}\left\{-\frac{q_0 q_k}{m_0 m_k}\frac{1}{r_k^3}(\mathbf{r}_k\times\mathbf{p}_l)\right.$$
$$\left.+\frac{q_k q_l}{2m_k}\frac{1}{r_{kl}^3}\left[\mathbf{r}_{lk}\times\left(\frac{1}{m_k}\mathbf{p}_k - \frac{2}{m_l}\mathbf{p}_l\right)\right]\right\}$$
$$\equiv \hat{H}_{\rm SO1} + \hat{H}_{\rm SO2}. \tag{11}$$

The operator can be split into the one-electron operator $\hat{H}_{\rm SO1}$ and the two-electron operator $\hat{H}_{\rm SO2}$. Both operators have a scalar-product structure involving a spin-vector operator and a spatial-vector operator. Thus, also in this case, the tensor operator techniques [34] are applied [25]. By setting the nuclear mass m_0 to infinity, the $\hat{H}_{\rm SO1}$ and $\hat{H}_{\rm SO2}$ terms in Eq. (11) become equal to the standard spin-orbit and spin-other-orbit interaction operators [27,35,36].

IV. VARIATIONAL CALCULATIONS

The variational nonrelativistic non-BO calculations of the eight considered ^3P states of beryllium, i.e., the $2s\,np$, $n = 2,\ldots,9$, ^3P states (the states are denoted as $n\,^3P$, $n = 2,\ldots,9$), are performed separately and independently for each state. In these calculations, the ECG basis set is grown for each state from a small set of functions to the final set. The procedure involves a series of additions of subsets of new functions (usually each subset contains 100 ECGs) and optimizing the exponential coefficients (i.e., the L_k matrix elements) separately for each function using the gradient-based variational optimization procedure. The optimization of the wave-function linear expansion coefficients is carried out by solving the secular equation. More details about the optimization procedure can be found in our previous work [25]. The growing of the basis set is performed using the FNM approach for the ^{9}Be isotope. Then, as mentioned, the basis sets are reused to perform infinite-nuclear-mass (INM) $^\infty$Be calculations.

The calculation of the SO and SS spatial matrix elements needed to calculate the SO and SS energy corrections were implemented in our previous work [25]. A detailed description of the algorithms can be found in that paper.

V. TOTAL ENERGY

After the nonrelativistic energies of the considered states are calculated, the spin-dependent relativistic effects are determined using the first-order perturbation theory, with the zero-order wave function being the nonrelativistic wave function of the particular state. The addition of the first-order relativistic corrections to the nonrelativistic energy uniformly shifts the $^3P_{J=0,1,2}$ energy levels by

$$E_{\rm rel}^{\rm shift} = E_{\rm MV} + E_{\rm D} + E_{\rm OO} + E_{\rm SSF}. \tag{12}$$

TABLE I. The convergence of the spin-free relativistic corrections of the order of α^2 and QED corrections of the orders of α^3 and α^4 (approximately) with the size of the basis set for the lowest eight ^3P states of beryllium (^{9}Be). The results for $^\infty$Be calculated with the largest basis sets are also shown. All values are in hartrees.

Isotope	Basis	$E_{\rm nrel}$[a]	$10^2\alpha^2$ MV	$10^2\alpha^2$ Darwin	$10^5\alpha^2$ OO	$10^3\alpha\,^2E_{\rm rel}{}^{\rm shift}$	$10^4\alpha\,^3E_{\rm QED}$	$10^5\alpha\,^4E_{\rm HQED}$
			$2\,^3P$					
^{9}Be	7000	−14.566341469	−1.41872	1.14030	−4.02327	−2.300225	3.34841	1.5215
^{9}Be	8000	−14.566341478	−1.41872	1.14030	−4.02327	−2.300226	3.34841	1.5215
^{9}Be	9000	−14.566341480	−1.41871	1.14030	−4.02327	−2.300163	3.34841	1.5215
$^\infty$Be	9000	−14.567244230	−1.41906	1.14052	−3.88411	−2.300079	3.34903	1.5217
			$3\,^3P$					
^{9}Be	7000	−14.398065853	−1.42716	1.14682	−4.84363	−2.323588	3.36818	1.5302
^{9}Be	8000	−14.398065860	−1.42716	1.14682	−4.84363	−2.323581	3.36818	1.5302
^{9}Be	9000	−14.398065863	−1.42716	1.14683	−4.84363	−2.323577	3.36819	1.5302
$^\infty$Be	9000	−14.398968692	−1.42751	1.14704	−4.70328	−2.323491	3.36881	1.5305
			$4\,^3P$					
^{9}Be	7000	−14.362049933	−1.42797	1.14748	−4.93329	−2.325521	3.37022	1.5311
^{9}Be	8000	−14.362049940	−1.42797	1.14748	−4.93329	−2.325530	3.37021	1.5311
^{9}Be	9000	−14.362049944	−1.42797	1.14749	−4.93329	−2.325556	3.37021	1.5311
$^\infty$Be	9000	−14.362951448	−1.42832	1.14770	−4.79281	−2.325469	3.37084	1.5314
			$5\,^3P$					
^{9}Be	8000	−14.347224126	−1.42819	1.14767	−4.96059	−2.326171	3.37076	1.5314
^{9}Be	9000	−14.347224128	−1.42820	1.14768	−4.96059	−2.326128	3.37079	1.5314
^{9}Be	10 000	−14.347224130	−1.42820	1.14768	−4.96059	−2.326092	3.37079	1.5314
$^\infty$Be	10 000	−14.348124994	−1.42855	1.14789	−4.82006	−2.326004	3.37141	1.5317
			$6\,^3P$					
^{9}Be	8000	−14.339637420	−1.42826	1.14772	−4.97180	−2.326301	3.37095	1.5314
^{9}Be	9000	−14.339637430	−1.42827	1.14772	−4.97180	−2.326310	3.37097	1.5314
^{9}Be	10 000	−14.339637441	−1.42827	1.14773	−4.97180	−2.326295	3.37096	1.5315
$^\infty$Be	10 000	−14.340537949	−1.42862	1.14794	−4.83126	−2.326208	3.37158	1.5317
			$7\,^3P$					
^{9}Be	8000	−14.335230926	−1.42817	1.14761	−4.97725	−2.326500	3.37065	1.5313
^{9}Be	9000	−14.335230932	−1.42831	1.14774	−4.97725	−2.326673	3.37100	1.5315
^{9}Be	10 000	−14.335230949	−1.42831	1.14774	−4.97725	−2.326669	3.37101	1.5315
$^\infty$Be	10 000	−14.336131240	−1.42867	1.14795	−4.83670	−2.326582	3.37164	1.5318
			$8\,^3P$					
^{9}Be	8000	−14.332444066	−1.42803	1.14741	−4.98022	−2.327015	3.37009	1.5310
^{9}Be	9000	−14.332444174	−1.42818	1.14757	−4.98022	−2.326982	3.37056	1.5313
^{9}Be	10 000	−14.332444254	−1.42820	1.14759	−4.98022	−2.326965	3.37062	1.5313
$^\infty$Be	10 000	−14.333344405	−1.42856	1.14780	−4.83967	−2.326878	3.37124	1.5316
			$9\,^3P$					
^{9}Be	8000	−14.330568921	−1.42800	1.14730	−4.98198	−2.327637	3.36983	1.5309
^{9}Be	9000	−14.330569470	−1.42801	1.14734	−4.98198	−2.327409	3.36992	1.5310
^{9}Be	10 000	−14.330569664	−1.42816	1.14748	−4.98198	−2.327576	3.37031	1.5311
$^\infty$Be	10 000	−14.331469717	−1.42851	1.14769	−4.84142	−2.327489	3.37094	1.5314

[a]Increasing the basis functions of states $2\,^3P$, $3\,^3P$, and $4\,^3P$ states to 10 000 ECGs gives nonrelativistic energies of ^{9}Be of −14.566341481, −14.398065864, and −14.362049945 a.u., respectively, and nonrelativistic energies of $^\infty$Be of −14.567244231, −14.398968693, and −14.362951450 a.u., respectively. Increasing the basis functions of states $8\,^3P$ and $9\,^3P$ states to 11 000 ECGs gives nonrelativistic energies of ^{9}Be of −14.332444310 and −14.330569811 a.u., respectively, and nonrelativistic energies of $^\infty$Be of −14.333344460 and −14.331469863 a.u., respectively.

The sum of the α^3 QED corrections also uniformly shifts the energy levels by [13,37]

$$E_{\rm QED} = \frac{4}{3}Z\left[\ln(\alpha^{-2}) + \frac{19}{30} - \ln k_0\right]\sum_{i=1}^{n}\langle\delta(\mathbf{r}_i)\rangle + \left(\frac{164}{15} + \frac{14}{3}\ln\alpha\right)\sum_{i>j=1}^{n}\langle\delta(\mathbf{r}_{ij})\rangle - \frac{14}{3}\frac{1}{4\pi}\sum_{i>j=1}^{n}\langle P\left(\frac{1}{r_{ij}^3}\right)\rangle \tag{13}$$

and by the value of the approximately calculated α^4 QED correction [13]:

$$E_{\rm HQED} = \pi Z^2\left(\frac{427}{96} - 2\ln 2\right)\sum_{i=1}^{n}\langle\delta(\mathbf{r}_i)\rangle. \tag{14}$$

Although the above two formulas were originally derived within the INM approach, they are calculated here using the FNM nonrelativistic wave functions. Thus, the recoil α^3 QED energy corrections is partially included in the calculation [38].

The total energies that include the spin-orbit and spin-spin energy corrections for the considered $^3P_{J=0,1,2}$ states of the beryllium atom are calculated as

$$E_J = E_{\rm nrel} + \alpha^2\left[E_{\rm rel}^{\rm shift} + C_J^{\rm SO}(E_{\rm SO1} + E_{\rm SO2}) + C_J^{\rm SS}E_{\rm SS}\right] + \alpha^3(E_{\rm QED} + E_\kappa) + \alpha^4 E_{\rm HQED}, \quad (15)$$

where the $C_J^{\rm S\bullet}$ coupling coefficients have the following values: $C^{\rm SO}_{J=0,1,2} = -2, -1, 1$ and $C^{\rm SS}_{J=0,1,2} = 10, -5, 1$. $E_{\rm SO1}$, $E_{\rm SO2}$, and $E_{\rm SS}$ are the expectation values of the respective operators as described in Ref. [25]. These expectation values are calculated using the wave functions representing the considered $|n\ ^3P\ M_S = 1,\ M_L = 1\rangle$ states, where $n = 2, 3, \ldots, 9$ for the beryllium atom. The algorithm for calculating the α^3 correction due to the anomalous magnetic moment of the electron κ ($\approx \frac{\alpha}{2\pi}$) was also shown in Ref. [25].

VI. RESULTS

In the present work, the following values were used: $\alpha = 7.2973525698(24) \times 10^{-3}$ and 1 hartree $= 2.194746313708(11) \times 10^5$ cm^{-1} [39]. The calculations were carried out with a computer program written in FORTRAN90 that employs the message-passing interface (MPI) protocol for parallel processing. The most time-consuming part of the calculations is growing and optimizing the ECG basis set for each of the considered eight ^3P states of ^{9}Be.

In Table I we present the results of the nonrelativistic energies and the leading J-independent relativistic and QED corrections for the eight lowest ^3P states of ^{9}Be. We should note that in the calculations of the QED corrections for the states we use the value of the Bethe logarithm ($\ln k_0 = 5.75232$ a.u.) calculated for state $2\ ^1P$ of $^\infty$Be taken from Ref. [16]. As pointed out in Ref. [25], the QED correction that includes the Bethe logarithm is rather insensitive to small changes in the value of $\ln k_0$, so its approximate constant value used in this work for all considered states should little affect the accuracy of the calculations. The spin-dependent energy terms, $E_{\rm SO1}$, $E_{\rm SO2}$, and $E_{\rm SS}$, are shown in Table II. These terms are the expectation values of the corresponding relativistic operators calculated for states $|n\ ^3P, M_S = 1, M_L = 1\rangle$, where $n = 2, \ldots, 9$. In both Tables I and II, the convergence in the terms with the number of basis functions calculated for ^{9}Be is shown. As one can see, all quantities are, in general, very well converged. Also, as one notices, the three quantities contributing to the fine line splitting quickly decrease with the increasing electronic-excitation level.

In the sixth column of Table I, the α^2 orbit-orbit relativistic correction is shown. We should point out that there was an error in the calculations for the orbit-orbit relativistic correction in our previous work [25], where the two lowest ^3P states of beryllium were considered. This error has been now corrected, and the values of the spin-independent relativistic correction shown in Table I include the corrected orbit-orbit term.

Before the results are analyzed, let us first compare the general splitting schemes of the ^3P atomic terms of the ^{9}Be atom presented in Fig. 1. As one can see, the splitting pattern is almost identical for all eight states, but energy scales are very different. The SO interaction in the $^3P_{J=0,1,2}$ energy levels results in the splitting pattern that follows the so-called Landé interval rule, which predicts the $(E_2 - E_1)/(E_1 - E_0) = 2$ splitting ratio. The SS interaction may affect this ratio, but in the case of ^{9}Be, the SS interaction is relatively small, and the Landé interval rule still applies. As in the present calculation we do not include the mixing of the triplet $^3P_1$ states with the closely lying $^1P_1$ singlet states, the slight downshifting of the $^3P_1$ states resulting from the triplet-singlet coupling is not described. We also do not include the higher-order QED corrections [38,40] that may slightly affect the fine structure of the beryllium ^3P states.

TABLE II. J-dependent relativistic corrections of the order of α^2 to the energy of the $n = 2, 3, \ldots, 9$ ^3P states of the beryllium atom (^{9}Be and $^\infty$Be). All values are in a.u.

Isotope	Basis	$\alpha^2 E_{\rm SO1}$ ($\times 10^5$)	$\alpha^2 E_{\rm SO2}$ ($\times 10^5$)	$\alpha^2 E_{\rm SS}$ ($\times 10^7$)
		$2\ ^3P$		
^{9}Be	7000	1.61224	−1.11247	1.364
^{9}Be	8000	1.61224	−1.11247	1.364
^{9}Be	9000	1.61224	−1.11247	1.364
$^\infty$Be	9000	1.61208	−1.11225	1.365
		$3\ ^3P$		
^{9}Be	7000	0.22948	−0.15453	0.210
^{9}Be	8000	0.22948	−0.15453	0.210
^{9}Be	9000	0.22948	−0.15453	0.210
$^\infty$Be	9000	0.22944	−0.15449	0.210
		$4\ ^3P$		
^{9}Be	7000	0.08428	−0.05629	0.072
^{9}Be	8000	0.08428	−0.05629	0.072
^{9}Be	9000	0.08428	−0.05628	0.072
$^\infty$Be	9000	0.08426	−0.05627	0.072
		$5\ ^3P$		
^{9}Be	8000	0.04036	−0.02686	0.034
^{9}Be	9000	0.04036	−0.02686	0.034
^{9}Be	10000	0.04036	−0.02686	0.034
$^\infty$Be	10000	0.04035	−0.02685	0.034
		$6\ ^3P$		
^{9}Be	8000	0.02242	−0.01489	0.018
^{9}Be	9000	0.02242	−0.01489	0.018
^{9}Be	10000	0.02242	−0.01489	0.018
$^\infty$Be	10000	0.02241	−0.01489	0.018
		$7\ ^3P$		
^{9}Be	8000	0.01372	−0.00911	0.011
^{9}Be	9000	0.01372	−0.00911	0.011
^{9}Be	10000	0.01372	−0.00911	0.011
$^\infty$Be	10000	0.01372	−0.00911	0.011
		$8\ ^3P$		
^{9}Be	8000	0.00901	−0.00597	0.007
^{9}Be	9000	0.00901	−0.00597	0.007
^{9}Be	10000	0.00901	−0.00597	0.007
$^\infty$Be	10000	0.00900	−0.00597	0.007
		$9\ ^3P$		
^{9}Be	8000	0.00623	−0.00413	0.005
^{9}Be	9000	0.00623	−0.00413	0.005
^{9}Be	10000	0.00623	−0.00413	0.005
$^\infty$Be	10000	0.00622	−0.00412	0.005

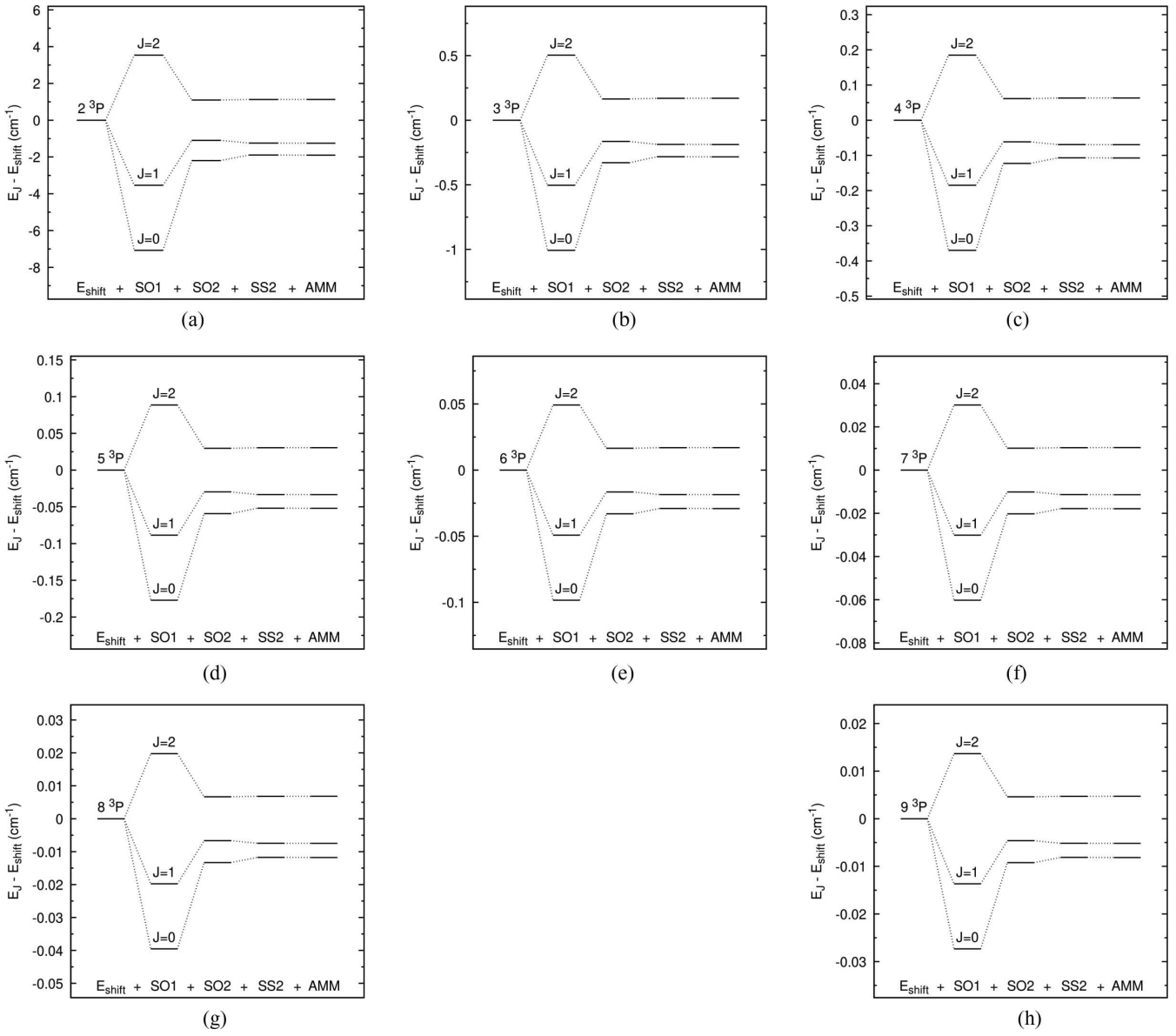

FIG. 1. Fine splitting of the $n\ ^3P$, $n = 2, \ldots, 9$, atomic term into $J = 0, 1, 2$ energy levels of the ^{9}Be atom due to spin-dependent α^2 relativistic interactions and due to the α^3 correction representing the effect of the anomalous magnetic moment of the electron (AMM). $E_{\rm shift} = E_{\rm nrel} + \alpha^2 E_{\rm rel}^{\rm shift} + \alpha^3 E_{\rm QED} + \alpha^4 E_{\rm HQED}$, E_J is defined in Eq. (15), and the SS2 term is obtained by subtracting from the expectation value of operator (10) a part of the spin-spin contact term (9), as described in the statement below Eq. (10). The splitting patterns are almost identical for all states, but as one can see in the plots, the energy scales are different. (a) State 2, (b) state 3, (c) state 4, (d) state 5, (e) state 6, (f) state 7, (g) state 8, and (h) state 9.

Table I shows the nonrelativistic energies are converged to a relative precision of 10^{-8}–10^{-9}. Thus, by taking into account the level of convergence of the relativistic and QED corrections and by accounting for the inaccuracy related to using an approximate value for the Bethe logarithm $\ln k_0$, we can estimate the absolute error of the total energies of the considered ^3P states to be not larger than roughly 2×10^{-6} a.u. $<$ 0.5 cm^{-1}. As can be seen in Table III, the $\alpha\,^3E_{QED}$ corrections are two orders of magnitude larger than this error upper bound, and even more important, these corrections differ by roughly 2×10^{-6} a.u. for the 2 ^3P and 3 ^3P states. This shows the importance of the QED corrections in the present calculations. The higher-order QED corrections in terms of α, e.g., the approximate α^4 QED terms taken into account in the present calculations, are expected to be of the order of about 1 cm^{-1}. Their impact on the transition energies is expected to be smaller than 0.1 cm^{-1} [13,15]; that is, it is below the estimated accuracy of the present calculations. The values of the $\alpha\,^4E_{\rm HQED}$ corrections are collected in Table I.

There are some experimental data that concern the total energies of the ^3P_J energy levels of beryllium determined with respect to the ground electronic ^1S state [1]. The available experimental energy values are compared with the values calculated in this work in Table III. As one can see, most of the total energies calculated in this work fall within the uncertainty brackets of the experimental values.

TABLE III. Total energies E_J of the $n\,^3P_J$, $n = 2, \ldots, 9$, of ^{9}Be (in a.u.) and the corresponding excitation energies (in cm^{-1}) determined with respect to the ^{9}Be ground-state energy of $-14.668440600(18)$ a.u. obtained with 16 000 ECG basis functions (the energy is taken from [41] and it includes the QED correction with the value of the Bethe logarithm taken from Ref. [16]). The excitation energies are compared with the experimental values [1]. The total E_J energies calculated for $^\infty$Be are also included. The calculations for the $2\,^3P_0$, $2\,^3P_1$, $2\,^3P_2$, $3\,^3P_0$, $3\,^3P_1$, $3\,^3P_2$, $4\,^3P_0$, $4\,^3P_1$, and $4\,^3P_2$ states are done with 9000 ECGs, and the calculations for the $5\,^3P_0$, $5\,^3P_1$, $5\,^3P_2$, $6\,^3P_0$, $6\,^3P_1$, $6\,^3P_2$, $7\,^3P_0$, $7\,^3P_1$, $7\,^3P_2$, $8\,^3P_0$, $8\,^3P_1$, $8\,^3P_2$, $9\,^3P_0$, $9\,^3P_1$, and $9\,^3P_2$ states are done with 10 000 ECGs. The E_J energies of the ^3P_J states of Be are calculated using Eq. (15). The calculated results are compared with the experimental values take from Ref. [1].

State	Isotope	E_J (a.u.)	E_J (cm^{-1})[b]	$E_{\text{exp.}}$ (cm^{-1})	ΔE_J [a] (cm^{-1})
$2\,^3P_0$	^{9}Be	−14.56830025(4)	21 978.266 ± 0.009	21 978.310 ± 0.080	−0.044
	$^\infty$Be	−14.56920285			
$2\,^3P_1$	^{9}Be	−14.56829729(4)	21 978.916 ± 0.009	21 978.310 ± 0.080	−0.009
	$^\infty$Be	−14.56919989			
$2\,^3P_2$	^{9}Be	−14.56828644(4)	21 981.297 ± 0.009	21 981.260 ± 0.070	0.037
	$^\infty$Be	−14.56918904			
$3\,^3P_0$	^{9}Be	−14.400038611(1)	58 907.427 ± 0.000	58 907.472 ± 0.060	−0.045
	$^\infty$Be	−14.400941289			
$3\,^3P_1$	^{9}Be	−14.400038176(1)	58 907.522 ± 0.000	58 907.472 ± 0.060	0.050
	$^\infty$Be	−14.400940854			
$3\,^3P_2$	^{9}Be	−14.400036546(1)	58 907.880 ± 0.000	58 907.839 ± 0.060	0.041
	$^\infty$Be	−14.400939223			
$4\,^3P_0$	^{9}Be	−14.36402366(2)	66 811.796 ± 0.004	66 811.890 ± 0.140	−0.094
	$^\infty$Be	−14.36492501			
$4\,^3P_1$	^{9}Be	−14.36402348(2)	66 811.834 ± 0.004	66 811.890 ± 0.090	−0.056
	$^\infty$Be	−14.36492484			
$4\,^3P_2$	^{9}Be	−14.36402288(2)	66 811.967 ± 0.004	66 811.890 ± 0.080	0.077
	$^\infty$Be	−14.36492423			
$5\,^3P_0$	^{9}Be	−14.34919807(4)	70 065.637 ± 0.004	70 065.400 ± 0.100	0.237
	$^\infty$Be	−14.35009878			
$5\,^3P_1$	^{9}Be	−14.34919798(4)	70 065.655 ± 0.004	70 065.400 ± 0.140	0.255
	$^\infty$Be	−14.35009869			
$5\,^3P_2$	^{9}Be	−14.34919769(4)	70 065.719 ± 0.004	70 065.400 ± 0.140	0.319
	$^\infty$Be	−14.35009840			
$6\,^3P_0$	^{9}Be	−14.34161146(1)	71 730.705 ± 0.002	71 730.640 ± 0.080	0.065
	$^\infty$Be	−14.34251181			
$6\,^3P_1$	^{9}Be	−14.34161141(1)	71 730.715 ± 0.002	71 730.660 ± 0.060	0.055
	$^\infty$Be	−14.34251177			
$6\,^3P_2$	^{9}Be	−14.34161125(1)	71 730.751 ± 0.002	71 730.660 ± 0.060	0.091
	$^\infty$Be	−14.34251160			
$7\,^3P_0$	^{9}Be	−14.33720528(8)	72 697.748 ± 0.018	72 697.330 ± 0.080	0.418
	$^\infty$Be	−14.33810542			
$7\,^3P_1$	^{9}Be	−14.33720525(8)	72 697.755 ± 0.018	72 697.340 ± 0.070	0.415
	$^\infty$Be	−14.33810539			
$7\,^3P_2$	^{9}Be	−14.33720515(8)	72 697.777 ± 0.018	72 697.340 ± 0.060	0.437
	$^\infty$Be	−14.33810529			
$8\,^3P_0$	^{9}Be	−14.33441898(4)	73 309.289 ± 0.009	73 309.170 ± 0.090	0.119
	$^\infty$Be	−14.33531890			
$8\,^3P_1$	^{9}Be	−14.33441887(4)	73 309.293 ± 0.009	73 309.160 ± 0.070	0.133
	$^\infty$Be	−14.33531888			
$8\,^3P_2$	^{9}Be	−14.33441881(4)	73 309.308 ± 0.009	73 309.150 ± 0.060	0.158
	$^\infty$Be	−14.33531881			
$9\,^3P_0$	^{9}Be	−14.3325449(3)	73 720.577 ± 0.066		
	$^\infty$Be	−14.3334448			
$9\,^3P_1$	^{9}Be	−14.3325449(3)	73 720.580 ± 0.066		
	$^\infty$Be	−14.3334448			
$9\,^3P_2$	^{9}Be	−14.3325449(3)	73 720.589 ± 0.066		
	$^\infty$Be	−14.3334448			

[a] $\Delta E_J = E_J - E_J^{\text{exp}}$, where experimental E_J^{exp} energies of Be taken from NIST [1].

[b] Ground state energy of ^{9}Be $E_g = E_{\text{nrel}} + \alpha^2 E_{\text{rel}}^{\text{shift}} + \alpha^3 E_{\text{QED}} + \alpha^4 E_{\text{HQED}}$ obtained for 16000 basis; QED terms $\ln k_0$ taken from Ref. [16].

TABLE IV. Fine E_J-$E_{J'}$ splitting (in cm^{-1}) of the lowest eight ^3P_J states of ^{9}Be. The calculated energy differences are compared with the experiment [1].

Basis	$E_1 - E_0$	$E_2 - E_1$
	$2\,^3P_J$	
7000	0.650	2.381
8000	0.650	2.381
9000	0.650	2.381
Expt.	0.615 ± 0.090	2.335 ± 0.080
	$3\,^3P_J$	
7000	0.096	0.358
8000	0.096	0.358
9000	0.096	0.358
Expt.	0.0 ± 0.120	0.367 ± 0.120
	$4\,^3P_J$	
7000	0.038	0.133
8000	0.038	0.133
9000	0.038	0.133
Expt.	0.0 ± 0.230	0.0 ± 0.170
	$5\,^3P_J$	
8000	0.019	0.064
9000	0.019	0.064
10 000	0.019	0.064
Expt.	0.0 ± 0.240	0.0 ± 0.280
	$6\,^3P_J$	
8000	0.011	0.036
9000	0.011	0.036
10 000	0.011	0.036
Expt.	0.020 ± 0.140	0.0 ± 0.120
	$7\,^3P_J$	
8000	0.007	0.022
9000	0.007	0.022
10 000	0.007	0.022
Expt.	0.010 ± 0.150	0.0 ± 0.130
	$8\,^3P_J$	
8000	0.004	0.014
9000	0.004	0.014
10 000	0.004	0.014
Expt.	-0.010 ± 0.160	-0.010 ± 0.130
	$9\,^3P_J$	
9000	0.003	0.010
10 000	0.003	0.010

In our previous work [25] we estimated the error arising from not including the effect of the coupling between the $n\ ^3P$ states and the most closely lying $n\ ^1P$ states due to the spin-orbit interactions. Considering the very good convergence of the quantities used in the present work to calculate the SO interactions and based on the error analysis presented in our previous work [25], we estimate the uncertainties in the calculated splitting to be about 10^{-3} cm^{-1}. The experimental uncertainties are much higher [1].

Finally, in Table IV, the differences between the energies of the $n\,^3P_1$ and $n\,^3P_0$ states and the $n\,^3P_2$ and $n\,^3P_1$ states for $n = 2, \ldots, 9$, calculated in this work are presented. The calculated values are compared with the available experimental data [1]. As one can see, apart from perhaps the two lowest levels, the experiment is rather incomplete and imprecise. The differences calculated for the two lowest levels are well within the experimental uncertainties. One can also see that the calculated energy differences are very well converged with the number of ECGs.

VII. SUMMARY

This work presented high-accuracy calculations of the eight lowest ^3P energy levels of beryllium. Large explicitly correlated all-electron Gaussian basis functions were used to expand the spatial parts of the wave functions of the studied states. The nonlinear parameters of the Gaussians were variationally optimized for each state by the minimization of the total nonrelativistic energy of the state. The optimization employed the energy gradient determined with respect to the parameters. The nonrelativistic energies were augmented with the leading relativistic and QED corrections. The main focus of the work was the calculations of the splitting of the ^3P energy levels arising from the spin-orbit magnetic interactions, i.e., the fine structure of the energy levels. For the few available experimental values of the splitting, the calculated results fall well within the experimental error brackets. For the levels for which the splitting has not been measured or has been measured imprecisely, the present results may provide useful information to future experiment remeasurement attempts.

In future work, the approach used in this work will be applied to states of larger atomic systems with a wider range of the L and S quantum numbers. Future work will also be done on extending the capability of the present approach to include algorithms to calculate the off-diagonal SO interactions, as well as the hyperfine interactions.

ACKNOWLEDGMENTS

This work has been supported by a grant from the National Science Foundation, Grant No. 1856702. L.A. acknowledges the support of the Centre for Advanced Study (CAS) in Oslo, Norway, which funds and hosts our research project, titled "Atto-second Quantum Dynamics Beyond the Born-Oppenheimer Approximation," during the 2021/2022 academic year. The authors are grateful to the University of Arizona Research Computing for providing computational resources for this work.

[1] A. E. Kramida, Yu. Ralchenko, J. Reader, and NIST ASD Team, NIST Atomic Spectra Database, version 5.6, NIST, Gaithersburg, MD, http://physics.nist.gov/asd.

[2] L. M. Wang, C. Li, Z.-C. Yan, and G. W. F. Drake, Phys. Rev. A **95**, 032504 (2017).

[3] P. J. Pelzl, G. J. Smethells, and F. W. King, Phys. Rev. E **65**, 036707 (2002).

[4] D. M. Feldmann, P. J. Pelzl, and F. W. King, J. Math. Phys. **39**, 6262 (1998).
[5] Z.-C. Yan, M. Tambasco, and G. W. F. Drake, Phys. Rev. A **57**, 1652 (1998).
[6] Z.-C. Yan, W. Nörtershäuser, and G. W. F. Drake, Phys. Rev. Lett. **100**, 243002 (2008).
[7] M. Puchalski and K. Pachucki, Phys. Rev. A **73**, 022503 (2006).
[8] F. W. King, D. Quicker, and J. Langer, J. Chem. Phys. **134**, 124114 (2011).
[9] M. Stanke, D. Kędziera, S. Bubin, and L. Adamowicz, Phys. Rev. Lett. **99**, 043001 (2007).
[10] S. Bubin, J. Komasa, M. Stanke, and L. Adamowicz, Phys. Rev. A **81**, 052504 (2010).
[11] S. Bubin, J. Komasa, M. Stanke, and L. Adamowicz, J. Chem. Phys. **132**, 114109 (2010).
[12] S. Bubin, M. Stanke, and L. Adamowicz, J. Chem. Phys. **131**, 044128 (2009).
[13] K. Pachucki and J. Komasa, Phys. Rev. Lett. **92**, 213001 (2004).
[14] K. Pachucki and J. Komasa, Phys. Rev. A **73**, 052502 (2006).
[15] M. Puchalski, J. Komasa, and K. Pachucki, Phys. Rev. A **87**, 030502(R) (2013).
[16] M. Puchalski, K. Pachucki, and J. Komasa, Phys. Rev. A **89**, 012506 (2014).
[17] M. Puchalski, J. Komasa, and K. Pachucki, Phys. Rev. A **92**, 062501 (2015).
[18] S. Bubin and L. Adamowicz, J. Chem. Phys. **128**, 114107 (2008).
[19] S. Bubin, M. Cafiero, and L. Adamowicz, *Advances in Chemical Physics*, edited by S. A. Rice (John Wiley & Sons, Ltd., 2005), Vol. 131, Chap. 6, https://doi.org/10.1002/0471739464.ch6.
[20] K. Strasburger, Phys. Rev. A **99**, 052512 (2019).
[21] K. Strasburger, Phys. Rev. A **99**, 069901(E) (2019).
[22] K. L. Sharkey, M. Pavanello, S. Bubin, and L. Adamowicz, Phys. Rev. A **80**, 062510 (2009).
[23] K. L. Sharkey and L. Adamowicz, J. Chem. Phys. **140**, 174112 (2014).
[24] M. Puchalski, J. Komasa, and K. Pachucki, Phys. Rev. A **104**, 022824 (2021).
[25] A. Kędziorski, M. Stanke, and L. Adamowicz, Chem. Phys. Lett. **751**, 137476 (2020).
[26] C. F. Fischer and G. Tachiev, At. Data Nucl. Data Tables **87**, 1 (2004).
[27] K. T. Chung and X.-W. Zhu, Phys. Rev A **48**, 1944 (1993).
[28] C. Chen, J. At. Mol. Opt. Phys. **2012**, 1 (2012).
[29] F. A. Matsen and R. Pauncz, *The Unitary Group in Quantum Chemistry* (Elsevier, 1986, Amsterdam).
[30] R. Pauncz, *Spin Eigenfunctions* (Plenum, 1979, New York).
[31] M. Hamermesh, *Group Theory and Its Application to Physical Problems* (Addison-Wesley, Reading, MA, 1962).
[32] M. Stanke, J. Komasa, S. Bubin, and L. Adamowicz, Phys. Rev. A **80**, 022514 (2009).
[33] J. Karwowski and S. Fraga, Can. J. Phys. **52**, 536 (1974).
[34] B. R. Judd, *Operator Techniques in Atomic Spectroscopy* (McGraw-Hill, NY, 1963).
[35] S. A. Alexander, S. Datta, and R. L. Coldwell, Phys. Rev. A **81**, 032519 (2010).
[36] H. Horie, Prog. Theor. Phys. **10**, 296 (1953).
[37] K. Pachucki and J. Komasa, Phys. Rev. A **68**, 042507 (2003).
[38] V. A. Yerokhin and K. Pachucki, Phys. Rev. A **81**, 022507 (2010).
[39] P. J. Mohr, B. N. Taylor, and D. B. Newell, Rev. Mod. Phys. **84**, 1527 (2012).
[40] K. Pachucki and V. A. Yerokhin, Phys. Rev. Lett. **104**, 070403 (2010).
[41] S. Nasiri, L. Adamowicz, and S. Bubin, J. Phys. Chem. Ref. Data **50**, 043107 (2021).